INTERNATIONAL JOURNAL OF RESEARCH IN MECHANICAL, MECHATRONICS AND AUTOMOBILE ENGINEERING (IJRMMAE)
ISSN: 2454-1435 (Print) | 2454-1443 (online)
Volume 8 Issue 4, January – March 2023 - www.ijrmmae.in – Pages 1-15

FABRICATION AND CHARACTERIZATION OF SUPER HARD NANO Ti-DLC COATING FOR MECHANICAL APPLICATIONS

Sivakumar G D[1], Rajkumar P R[1*], Anwar Mohamed S[2], Vijayarasu I[1]

[1] Department of Mechanical Engineering, Sethu Institute of Technology, Pulloor, Kariapatti – 626115, India.

[2] UG Student, Department of Mechanical Engineering, Sethu Institute of Technology, Pulloor, Kariapatti – 626115, India.

*e-mail: prrajkumar@sethu.ac.in

Abstract

A closed field balanced magnetron sputtering system is used to deposit Ti doped DLC coated on stainless steel disks and micro-drills. The microstructures of the various coatings are analyzed using scanning electron microscope, while the coefficient of friction is analyzed using block on ring wear tester. The drilling performance of the coated micro-drills is evaluated by conducting high-speed through-hole drilling tests using Stainless steel plate specimens. The service life of the coated micro-drills is assessed utilizing different criteria, namely surface roughness of the drilled hole, and the wear of the cutting edge, respectively. Overall, the results show that the Ti doped DLC coating has the optimal high-speed machining performance, i.e. it extends the tool life by a factor of at least four compared to the uncoated micro-drill and yields a significant improvement in the machining quality.

Keywords: General Characterization, Nano structured Ti-DLC coating, Magnetron Sputtering

INTRODUCTION

Composites are made from two or more distinct materials that when combined are better (stronger, tougher, and/or more durable) than each would be separately. The word usually refers to the fiber-reinforced metal, polymer, and ceramic materials that were originally developed for aerospace use in the 1950s. Although composites are a "high-technology" development, to some extent they mimic the features of living organisms such as the microstructures of wood and bio-ceramics like mollusk shells. The fibers and matrix of advanced composites may be combined using a variety of fabrication processes, with the choice depending on the desired alignment of fibers, the number of parts to be produced, the size and complexity of the parts, and so on. Perhaps best known for their use in aerospace applications, advanced composites are also used by the automotive, biomedical, and sporting goods markets. In addition, these strong, stiff, lightweight materials are seeing increased use in the rehabilitation, repair, and retrofit of civil infrastructure--including, for example, as replacement bridge decks and wrapping for concrete columns.

INTERNATIONAL JOURNAL OF RESEARCH IN MECHANICAL, MECHATRONICS AND AUTOMOBILE ENGINEERING (IJRMMAE)
ISSN: 2454-1435 (Print) | 2454-1443 (online)
Volume 8 Issue 4, January – March 2023 - www.ijrmmae.in – Pages 1-15

CARBON-OVER VIEW

Carbon is a unique and abundant chemical element in nature and also proven to be one of the most fascinating elements. Carbon has an outstanding ability to form different hybridizations (sp3, sp2 and sp1). Depending on the hybridization, carbon can form structures of various geometries with different fractions of sp3 and sp2 bonding in both crystalline and non-crystalline forms. Diamond and graphite are the well-known crystalline forms of carbon, for which the structure and the properties are well understood. Recently, very important and great advances in the science of carbon have been developed in nano science and nanotechnology like PVD of diamond, discovery of C60 and carbon nanotubes. In Parallel to the crystalline carbon there was an equivalent development in the field of non-crystalline carbon and their deposition techniques. Glassy carbon, DLC film, carbon fibers, etc., are the non-crystalline forms of carbon, which are amorphous containing a mixture of sp3 and sp2 bonded carbon and has the properties between diamond and graphite.

DLC FILMS - AN OVERVIEW

DLC film is a met-stable form of amorphous carbon containing significant amount of sp3 bonds. It can be deposited as thin films over a range of surfaces using various techniques rather than any other forms.

Classification of Amorphous Carbon

In general, amorphous carbon is a mixture of sp3, sp2 and sp1 bonds in various proportions. The hydrogen content as well as sp2 to sp3 ratio determines the structure and properties of the DLC films obtained and this depends on the parameters of the deposition method employed. DLC films cane broadly classified into two broad categories as hydrogen free amorphous carbon (a-C) and hydrogenated amorphous carbon (a-C:H) based on the carbon source used for their deposition

DLC films formed only using solid carbon sources are termed as hydrogen-free DLC or non-hydrogenated DLC. Within this category a film rich in sp3 bonds (typically >70%) is denoted as tetrahedral amorphous carbon.

(**ta-C**) and this is obtained when the deposition densities are around 3 g/cm^2.At lower densities (< 2 g/ cm^2), the film has predominantly sp2 bonding [16]and it is termed as amorphous carbon (a-C).

The second category of DLC is obtained when the deposition is carried out using hydrocarbons precursors and they are termed as hydrogenated amorphous carbon or hydrogenated DLC (DLC:H), which contain a significant amount of hydrogen (approximately up to 50 atomic percent). These films are further classified into four major groups as follows a-C:H films with the highest H content (40–50%) are termed as polymer-like a-C:H (PLCH). These films can have up to ~60% sp3. However, most of the sp3 bonds are hydrogen terminated and these materials are soft (low density).

a-C:H films with intermediate H content (20–40%) are termed as diamond-like a-C:H (DLC:H). Even if these films have lower sp3 content, they form more C-C sp3 bonds when compared with PLCH. Thus, they have better mechanical properties.

Hydrogenated tetrahedral amorphous carbon films (ta-C:H).ta-C:H films are a class of DLC:H for which the C-C sp3 content can be increased while keeping a fixed H content. Thus, most films defined in literature as ta-C:H are just DLC:Hs. However, the ta-C:H films with the highest sp3 content (~70%) and ~25 atm.% H content do really fall in a different category.

a-C:H with low H content (less than 20%) are termed as graphite-like a-C:H (GLCH) and they have high

INTERNATIONAL JOURNAL OF RESEARCH IN MECHANICAL, MECHATRONICS AND AUTOMOBILE ENGINEERING (IJRMMAE)
ISSN: 2454-1435 (Print) | 2454-1443 (online)
Volume 8 Issue 4, January – March 2023 - www.ijrmmae.in – Pages 1-15

sp2 content and sp2 clustering.

DEPOSITION TECHNIQUES OF DLC FILMS;

Chemical vapor deposition

- Plating
- Chemical solution deposition
- Spin coating
- Chemical vapor deposition
- Plasma enhanced CVD
- Atomic layer deposition

Physical vapor deposition

- Thermal evaporator
- electron beam evaporator
- molecular beam epitaxial
- Sputtering
- Pulsed laser deposition
- Cathode arc deposition

PVD PROCESS;

The physical vapor deposition method is demonstrated in the following Figure 1.

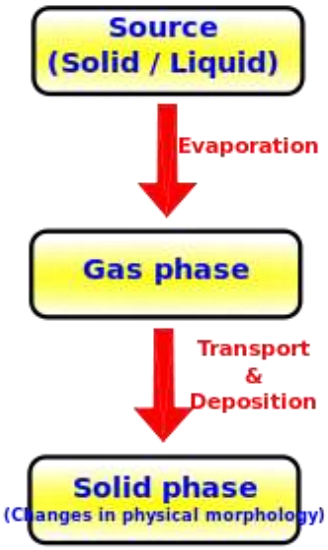

Fig 1.PVD process

ISSN: 2454-1435 (Print) | 2454-1443 (online)
Volume 8 Issue 4, January – March 2023 - www.ijrmmae.in – Pages 1-15

The coating method involves purely physical processes such as high-temperature vacuum evaporation with subsequent condensation, or plasma sputter bombardment rather than involving a chemical reaction at the surface to be coated as in chemical vapor deposition. PVD describes a variety of vacuum deposition methods used to deposit thin films by the condensation of a vaporized form of the desired film material onto various work piece surfaces (e.g., Si wafer). Physical vapor deposition coating is a product that is currently being used to enhance a number of products, including automotive parts like wheels and pistons, surgical tools, drill bits, and guns.

FOUR STEPSINVOLVED INPVD PROCESSES:

EVAPORATION

During this stage, a target, consisting of the material to be deposited is bombarded by a high energy source such as a beam of electrons or ions. This dislodges atoms from the surface of the target, 'vaporizing' them.

TRANSPORT

This process simply consists of the movement of 'vaporised' atoms from the target to the substrate to be coated and will generally be a straight line affair.

REACTION

In some cases coatings will consist of metal oxides, nitrides, carbides and other such materials. In these cases, the target will consist of the metal. The atoms of metal will then react with the appropriate gas during the transport stage. For the above examples, the reactive gases may be oxygen, nitrogen and methane.In instances where the coating consists of the target material alone, this step would not be part of the process.

DEPOSITION

This is the process of coating build up on the substrate surface Depending on the actual process, some reactions between target materials and the reactive gases may also take place at the substrate surface simultaneously with the deposition process.

OVER VIEW OF MAGNETRON SPUTTERING DEPOSITION;

A common technique used for many coating processes, in which the high energetic argon ions bombard the graphite electrodes to deposit DLC films. Plasma is generated by using either a DC or RF power. Pure carbon plasma with a broad energy distribution is produced by the impingement of the energetic ions on the graphitic target. A combination of hydrogen or CH_4 plasma with the Ar plasma results in hydrogenated DLC (a-C:H), whereas for it originated DLC nitrogen replaces either hydrogen or Ar. The drawbacks of this process, such as low deposition rates, low ion efficiencies in the plasma and the high substrate heating effects, can be overcome by the magnetron sputtering process. Here the magnets placed behind the target increases the path length of the electrons by giving them a spiral motion, thereby increasing the degree of ionization of the plasma and the resultant yield. The unbalanced magnetron and ion assisted deposition processes are the improvements of the sputtering techniques for obtaining high density films.

INTERNATIONAL JOURNAL OF RESEARCH IN MECHANICAL, MECHATRONICS AND AUTOMOBILE ENGINEERING (IJRMMAE)
ISSN: 2454-1435 (Print) | 2454-1443 (online)
Volume 8 Issue 4, January – March 2023 - www.ijrmmae.in – Pages 1-15

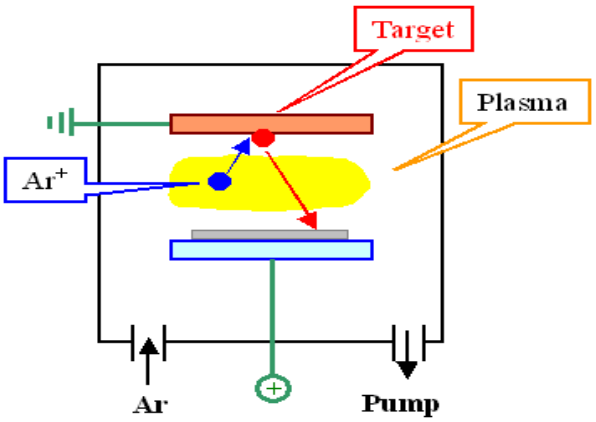

Fig 2. Schematic Diagram of sputtering

LITERATURE REVIEW

J. Takadoum et al, 2003explained the Diamond-like carbon and carbon nitride films were deposited on high speed steel substrates by plasma enhanced chemical vapour deposition technique. X-ray photoelectron spectroscopy and Fourier transform infrared spectroscopy were used to investigate the different bondings. Adhesion of the films to the substrate was investigated by the scratch test technique. The mechanical properties were investigated by nano-indentation and the tribologicalbehaviours were tested using a ball-on-disk tribometer. Effect of annealing on adhesion and mechanical properties was also investigated.

Yong Seob Parka et al, 2004explained the thin films of amorphous carbon (a-C) generally combine high wear resistance with low friction coefficients. In this study, the amorphous carbon (a-C) films are deposited on silicon with a close field unbalanced magnetron (CFUBM) sputtering system. The experimental data are obtained on the deposition rate and tribological properties of a-C films using DC bias voltage. The films are analyzed by Raman spectroscopy and AFM (atomic force microscopy). The tribological properties are investigated by hardness and friction coefficient measurements.

C. Corbella, et al, 2007clearly explainedThe relationship between metal-induced (W, Mo, Nb and Ti) structures and the surface properties of Me–DLC thin films is discussed. Nanocomposite films were deposited on c–Si wafers by pulsed-DC reactive magnetron sputtering controlling the gas ratio CH_4/Ar. The sputtering process of metals such as Ti, Nb and Mo (unlike the tungsten) in the presence of methane shows a low reactivity at low methane concentration. The deposition rate and the spatial distribution of sputtered material depend of *Z-ratio* of each metal. The surface contamination of metal targets by carbon, owing to methane dilution, limits the incorporation of metals into DLC films according to an exponential decay. Results of electron probe microanalysis and X-ray photoelectron spectroscopy indicate a C rich Me/C composition ratio for low relative methane flows.. This study shows the possibilities of controlling the amorphous carbon films structure and surface properties by introducing metal in the DLC matrix.

ISSN: 2454-1435 (Print) | 2454-1443 (online)
Volume 8 Issue 4, January – March 2023 - www.ijrmmae.in – Pages 1-15

M. Sedlaček, et al, 2008 investigated that due to their good wear resistance and low friction coefficient diamond-like carbon (DLC) coatings have been studied intensively for many years and a great deal of research has been carried out in the field of tribology. To facilitate an overview and comparison of the research results, a database containing information on the mechanical and tribological properties of coatings and base materials as well as the test conditions has been designed. The database is constructed in such a way that new data can be added easily. Practicability of the database has been checked on pin-on-disc contact tests using different contact conditions. The main purpose in building the database has been to examine the scientific and the practical value of the numerous research results on DLC coatings and to find out to what extent these data are comparable with one another. The analysis of the database has showed that it enables a fast search and comparison between different research results.

Jianmin Chen et al, 2008investigated the influence of hydrogen on the variation of mechanical properties and microstructure of diamond-like carbon (DLC) films synthesized by radio frequency plasma chemical vapor deposition (r.f.-PECVD). The DLC films were deposited on a silicon substrate (*p*-type). The reactant gases employed in this paper are a mixture of acetylene and hydrogen. The ratio of hydrogen in the gas mixture was successively varied to clarify its influence on the roughness, thickness, microstructure, hardness, modulus, residual stress and wear depth for the DLC films. The results reveal that increasing the concentration of hydrogen decreases thickness and roughness. Meanwhile, increasing the hydrogen concentration causes the decrease of sp^3 ratio, hardness as well as modulus. Finally, wear behavior is correlated to the surface morphology and hydrogen concentration for deposition with hydrogen-containing reactant gas.

Fei Zhao et al, 2010 clearly explained the Ti-doped hydrogenated DLC films were prepared by radio frequency sputtering. It was found that, after the incorporation of Ti together with O, the DLC films exhibit superior friction performance, including ultralow and steady friction coefficients (about 0.008) in ambient air, littlesensitivity to relative humidity and independence of counterpart material and test atmosphere. A combined effect of the inherent physical properties with the friction-induced structural transformation, and the presence of a transfer film, may explain the excellent lubrication performance of the Ti-DLC films.

S. Gayathri et al, 2012 investigated the tribological and scratch resistance properties of pulsed laser deposited Diamond-Like Carbon (DLC) coatings with transition metal interlayers (TM=Cr, Ag, Ti and Ni) are studied. Remarkably high scratch resistance property is found when DLC is deposited with Ni and Ti transition metal interlayer. Transformation of I(D)/I(G) ratio from a higher value on the surface to a lower value in the wear track of DLC indicates formation of graphitized/amorphizedtribofilm during sliding. These tribofilms and formation of carbonaceous transfer layer is a characteristic of easy in-plane sliding which provides low friction coefficient for the system of DLC/Ni and DLC/Ti multilayer.

Jinfeng Cui et al, 2014 explainedthe Ti-doped diamond-like carbon (DLC) films were deposited on Si substrates at room temperature by magnetron sputtering Ti twin-target in methane and argon mixture atmosphere. The DLC films with different Ti concentrations were fabricated by varying the gas flow ratio of Ar/CH_4. As a result, the hardness is decreased, while the stress is dramatically increased. The Ti-DLC films with 0.41% Ti doping showed a relatively high hardness (13.75 GPa), low stress (0.56 GPa), extremely low wear rate ($\sim 10^{-10}$ mm^3/Nm) and low friction coefficient (0.05)

ISSN: 2454-1435 (Print) | 2454-1443 (online)
Volume 8 Issue 4, January – March 2023 - www.ijrmmae.in – Pages 1-15

Yanxia Wu et al, 2014 investigated the (Ti)/diamond-like carbon (DLC) nanocomposite films with different Ti concentrations ranging from 0 to 11.02 at.% were prepared by medium frequency unbalanced magnetron sputtering, in which the mixed Ar/CH_4 of different volume ratios were used as the source gases. The doping effects of Ti concentration on microstructure, mechanical and vacuum tribological properties of the DLC films were investigated. It is found that the Ti concentration increased with the increasing Ar/CH_4 ratios, accompanied with the increasing number and size of Ti crystalline. With moderate incorporation of Ti at 3.55 at.%, the film (deposited at the Ar/CH_4 = 65/45) maintained a low internal stress without considerable decrease of hardness and thus improved the adhesion strength. Moreover, the film showed low friction coefficient and the longest sliding lifetime in vacuum. The significant improvement in tribological properties of TI/DLC nanocomposite films with moderate Ti concentration can be attributed to the low shear strength of Ti clusters on the surface, as well as the diffusion of Ti from the bulk to the surface and wear track.

W.H. Kao et al, 2012 explained the closed field unbalanced magnetron (CFUBM) sputtering system is used to deposit Zr–C:HN*x*% coatingswith nitrogen contents ranging from0 to 25 at.% onM2steel disks and micro-drills. The microstructures of the various coatings are analyzed using Raman spectrometry, while the hardness and adhesion strength are measured by performing nanoindentation tests and scratch tests, respectively. The drilling performance of the coated micro-drills is evaluated by conducting high-speed through-hole drilling tests using printed circuit board (PCB) specimens. The service life of the coated micro-drills is assessed utilizing four different criteria, namely the nail head ratio and surface roughness of the drilled hole, and the cornerwear and flank wear of the cutting edge, respectively. Overall, the results show that the Zr–C:H:N17% coating has the optimal high-speed machining performance, i.e. it extends the tool life by a factor of at least four compared to the uncoated micro-drill and yields a significant improvement in the machining quality.

H.Y. Ueng et al, 2014explained The Ti/TiN/TiCN/DLC multilayer coating on the microdrill was processed in a hybrid PVD-ECRCVD coating system. Functionally gradient Ti/TiN/TiCN supporting multilayer was pre-deposited initially on the microdrill in order to improve the adhesion strength of the DLC films. The following dry lubricant coating on it is composed of amorphous, diamondlikecarbon (DLC) deposited by ECRCVD plasma in the same recipient. For drilling applications, the combination of hard/softcoating layers, TiN/TiCN/DLC, allows it to improve chip flow with a lowered coefficient of friction and reduced cutting force. Inview of further cost reduction, technically the Ti/TiN/TiCN/DLC multilayer coating on microdrill could serve this purpose best.Functionally, in adapting a microdrill coated with DLC film, the quality of hole after inspection was found sufficiently superiorthan that of uncoated ones, and the drilling lifetime obtained a significant improvement reaching about 2.5 times

Zahra Khalaj et al, 2014 investigated the diamond-like carbon (DLC) films has been devoted to find both optimized conditions and characteristics of the deposited films on various substrates. In the present work, we investigate the quality of the DLC films grown on stainless steel substrates using different thickness of the nickel nanoparticle layers on the surface. Nickel nanoparticles were sputtered on the stainless steel substrates at 200 °C by a DC-sputtering system to make a good adherence between DLC coating and steel substrates. Diamond like carbon films were deposited on stainless steel substrates coated by nickel using pure acetylene and C2H2/H2 with 15% flow ratio by DC-Plasma Enhanced Chemical Vapor Deposition (PECVD) systems. Microstructural analysis by Raman spectroscopy showed a

ISSN: 2454-1435 (Print) | 2454-1443 (online)
Volume 8 Issue 4, January – March 2023 - www.ijrmmae.in – Pages 1-15

low intensity ratio ID/IG for DLC films by increasing the Ni layer thickness on the stainless steel substrates. Fourier Transforms Infrared spectroscopy (FTIR) evidenced the peaks attributed to C–H bending and stretching vibration modes in the range of 1300–1700 cm–1 and 2700–3100 cm–1, respectively, in good agreement with the Raman spectroscopy and confirmed the DLC growth in all samples.

Experimental Procedure

SUBSTRATE CLEANING PROCESS

CLEANING OF STAINLESS STEEL TOOL

The first step in cleaning of stainless steel surface (15 × 15 mm) was to sonicate using acetone. Acetone removes oil and other moisture on the steel surface.

COATING DEPOSITION

After substrate cleaning process, the coatings were deposited on stainless steel disks and 1mm micro-drills using a closed field balanced magnetron sputtering system (HIND HIVAC, Bangalore) with a single Titanium target, single graphite target and CH_4 as the reactive gas. In first process the DLC was deposited on the disk and the drill bits. The second process Ti doped DLC was deposited on another disk and drill bits. The conditions for the deposition process are shown in below (Table 1.).

S. No.	arget material	Sputtering/ Reactive gas	Material	Chamber pressure	Power (W)	Substrate temperature
1	Graphite	Ar /CH_4	SS plate & drill bits	$2x10^{-3}$	89	RT
2	Ti/Graphite	Ar /CH_4	S plate& drill bits	$3x10^{-3}$	90	RT

Table 1. Experimental Detail

Raman spectroscopy

Raman spectroscopy is a highly versatile technique that provides a simple, fast and non-destructive analysis of both organic and inorganic chemicals. Raman spectroscopy is a type of molecular spectroscopy that involves the dispersion of electromagnetic radiation by molecules or atoms. It measures the rotational, vibrational, and other low-frequency modes of molecules.

Raman spectroscopy offers several advantages. For instance, this technique is nondestructive and needs little or sample preparation. In fact, Raman analysis can be conducted directly via glasses, jars, plastic bags, cuvettes, and other transparent containers. Moreover, Raman can be used for qualitative as well as quantitative analysis.

This technique is highly selective, which means that it can easily differentiate molecules in chemicals that are very similar. Raman instrumentation is compact, portable and user-friendly. Even a nontechnical user can perform the analysis and quickly obtain the data, thus enabling first responders to adopt suitable precautions depending on the type of materials being searched on the scene.

Raman Spectrometer

A Raman spectrometer includes three main components such as the laser, the sampling interface, and the spectrometer itself. A typical Raman laser will consists of different characteristics, such as a small form factor, low power consumption, narrow linewidth, a stable power output, and a stable

INTERNATIONAL JOURNAL OF RESEARCH IN MECHANICAL, MECHATRONICS AND AUTOMOBILE ENGINEERING (IJRMMAE)
ISSN: 2454-1435 (Print) | 2454-1443 (online)
Volume 8 Issue 4, Jan. – Mar. 2023 - www.ijrmmae.in – Pages 1-15
Published On: 14th Feb 2023

wavelength output. In case Raman measurements are conducted using a 785nm source, it is important to ensure that the source is only emitting 785nm.

The second component includes the sampling interface. In many Raman spectrometers, fiber-optic probe is typically used which offers an extremely flexible sampling interface. These fiber-optic probes can be easily adapted to a range of optical microscopes, gas flow cells, liquid flow cells, and other sampling chambers. One critical aspect of a fiber-optic probe is a high-optical-density Raman cutoff. This means, when users are looking at the Raman spectrum, they need to ensure that the laser wavelength is blocked as much as possible so that the Raman shift can be observed. It is extremely important that the Raman shift is observed very close to the laser line since many materials have vital spectral features very near to the line.

The third component is the spectrometer. Here, important performance factors are small form factor, high resolution, low power consumption, and low noise. An appropriate detector is very important and must be utilized depending on which excitation laser is being used. For visible excitation, a standard CCD is selected; for UV excitation, a photomultiplier tube (PMT) or CCD is typically chosen; and for NIR excitation, an indium gallium arsenide (InGaAs) array is normally employed.

Fig 3. Raman spectroscopy

SEM ANALYSIS

A Scanning Electron Microscope (**SEM**) is a type of electron microscope that produces images of a sample by scanning it with a focused beam of electrons. The electrons interact with atoms in the sample, producing various signals that can be detected and that contain information about the sample's surface topography and composition. SEM can achieve resolution better than 1 nanometer. Specimens can be observed in high vacuum, in low vacuum, and (in environmental SEM) in wet conditions.

The types of signals produced by a SEM include secondary electrons (SE), back-scattered electrons (BSE), characteristic X-rays, light (cathode luminescence) (CL), specimen current and transmitted electrons. Secondary electron detectors are standard equipment in all SEMs, but it is rare that a single machine would have detectors for all possible signals. In the most common or standard detection mode, secondary electron imaging or SEI, the SEM can produce very high-resolution images of a sample surface, revealing details less than 1 nm in size. Due to the very narrow electron

INTERNATIONAL JOURNAL OF RESEARCH IN MECHANICAL, MECHATRONICS AND AUTOMOBILE ENGINEERING (IJRMMAE)
ISSN: 2454-1435 (Print) | 2454-1443 (online)
Volume 8 Issue 4, Jan. – Mar. 2023 - www.ijrmmae.in – Pages 1-15
Published On: 14th Feb 2023

beam, SEM micrographs have a large depth of field yielding a characteristic three-dimensional appearance useful for understanding the surface structure of a sample. This is exemplified by the micrograph of pollen shown above. A wide range of magnifications is possible, from about 10 times (about equivalent to that of a powerful hand-lens) to more than 500,000 times, about 250 times the magnification limit of the best light microscopes.

Back-scattered electrons (BSE) are beam electrons that are reflected from the sample by elastic scattering. BSE are often used in analytical SEM along with the spectra made from the characteristic X-rays, because the intensity of the BSE signal is strongly related to the atomic number (Z) of the specimen. BSE images can provide information about the distribution of different elements in the sample. For the same reason, BSE imaging can image colloidal gold immune-labels of 5 or 10 nm diameters, which would otherwise be difficult or impossible to detect in secondary electron images in biological specimens. Characteristic X-rays are emitted when the electron beam removes an inner shell electron from the sample, causing a higher-energy electron to fill the shell and release energy. These characteristic X-rays are used to identify the composition and measure the abundance of elements in the sample.

SCANNING PROCESS AND IMAGE FORMATION

At the top of the Fig 4.is the column where the electron beam is generated and focused. From the column comes the electron beam, also called the primary electrons, shown here as x-ray. When the primary electrons impact the surface they generate secondary electrons, backscattered electrons, Auger electrons, X-ray photons and cathode luminescence. The electron beam, which typically has an energy ranging from 0.2 keV to 40 keV, is focused by one or two condenser lenses to a spot about 0.4 nm to 5 nm in diameter. The beam passes through pairs of scanning coils or pairs of deflector plates in the electron column, typically in the final lens, which deflect the beam in the *x* and *y* axes so that it scans in a raster fashion over a rectangular area of the sample surface.

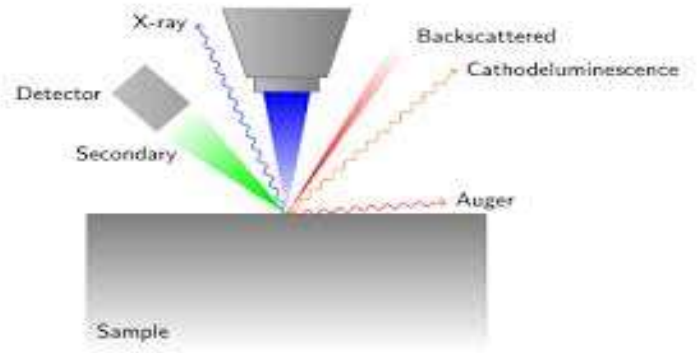

Fig 4. Mechanism of Scanning Electron Microscope

When the primary electron beam interacts with the sample, the electrons lose energy by repeated random scattering and absorption within a teardrop-shaped volume of the specimen known as the interaction volume, which extends from less than 100 nm to approximately 5 µm into the surface. The size of the interaction volume depends on the electron's landing energy, the atomic number of the specimen and the specimen's density. The energy exchange between the electron beam and the sample results in the reflection of high-energy electrons by elastic scattering, emission of secondary electrons by inelastic scattering and the emission of electromagnetic radiation, each of which can be detected by specialized detectors. The beam current absorbed by the specimen can also be detected

ISSN: 2454-1435 (Print) | 2454-1443 (online)
Volume 8 Issue 4, Jan. – Mar. 2023 - www.ijrmmae.in – Pages 1-15
Published On: 14th Feb 2023

and used to create images of the distribution of specimen current. Electronic amplifiers of various types are used to amplify the signals, which are displayed as variations in brightness on a computer monitor (or, for vintage models, on a cathode ray tube). Each pixel of computer videomemory is synchronized with the position of the beam on the specimen in the microscope, and the resulting image is therefore a distribution map of the intensity of the signal being emitted from the scanned area of the specimen. In older microscopes image may be captured by photography from a high-resolution cathode ray tube, but in modern machines image is saved to computer data storage.

The most common imaging mode collects low-energy (<50 eV) secondary electrons that are ejected from the k-shell of the specimen atoms by inelastic scattering interactions with beam electrons. Due to their low energy, these electrons originate within a few nanometers from the sample surface. The electrons are detected by an Everhart-Thorley detector, which is a type of scintillator-photomultiplier system. The secondary electrons are first collected by attracting them towards an electrically biased grid at about +400 V, and then further accelerated towards a phosphor or scintillate positively biased to about +2,000 V. The accelerated secondary electrons are now sufficiently energetic to cause the scintillate to emit flashes of light (cathode luminescence), which are conducted to a photomultiplier outside the SEM column via a light pipe and a window in the wall of the specimen chamber. The amplified electrical signal output by the photomultiplier is displayed as a two-dimensional intensity distribution that can be viewed and photographed on an analogue video display, or subjected to analog-to-digital conversion and displayed and saved as a digital image. This process relies on a raster-scanned primary beam. The brightness of the signal depends on the number of secondary electrons reaching the detector. If the beam enters the sample perpendicular to the surface, then the activated region is uniform about the axis of the beam and a certain number of electrons "escape" from within the sample. As the angle of incidence increases, the "escape" distance of one side of the beam will decrease, and more secondary electrons will be emitted. Thus steep surfaces and edges tend to be brighter than flat surfaces, which results in images with a well-defined, three-dimensional appearance. Using the signal of secondary electrons image resolution less than 0.5 nm is possible.

Backscattered electrons (BSE) consist of high-energy electrons originating in the electron beam that are reflected or back-scattered out of the specimen interaction volume by elastic scattering interactions with specimen atoms. Since heavy elements (high atomic number) backscatter electrons more strongly than light elements (low atomic number), and thus appear brighter in the image, BSE are used to detect contrast between areas with different chemical compositions. The Everhart- Thornley detector, which is normally positioned to one side of the specimen, is inefficient for the detection of backscattered electrons because few such electrons are emitted in the solid angle subtended by the detector, and because the positively biased detection grid has little ability to attract the higher energy BSE. Dedicated backscattered electron detectors are positioned above the sample in a "doughnut" type arrangement, concentric with the electron beam, maximizing the solid angle of collection. BSE detectors are usually either of scintillator or of semiconductor types. When all parts of the detector are used to collect electrons symmetrically about the beam, atomic number contrast is produced. However, strong topographic contrast is produced by collecting back-scattered electrons from one side above the specimen using an asymmetrical, directional BSE detector; the resulting contrast appears as illumination of the topography from that side. Semiconductor detectors can be made in radial segments that can be switched in or out to control the type of contrast produced and its directionality. Backscattered electrons can also be used to form electron backscatter diffraction (EBSD) image that can be used to determine the

INTERNATIONAL JOURNAL OF RESEARCH IN MECHANICAL, MECHATRONICS AND AUTOMOBILE ENGINEERING (IJRMMAE)
ISSN: 2454-1435 (Print) | 2454-1443 (online)
Volume 8 Issue 4, Jan. – Mar. 2023 - www.ijrmmae.in – Pages 1-15
Published On: 14th Feb 2023

crystallographic structure of the specimen.

The spatial resolution of the SEM depends on the size of the electron spot, which in turn depends on both the wavelength of the electrons and the electron-optical system that produces the scanning beam. The resolution is also limited by the size of the interaction volume, or the extent to which the material interacts with the electron beam. The spot size and the interaction volume are both large compared to the distances between atoms, so the resolution of the SEM is not high enough to image individual atoms, as is possible in the shorter wavelength (i.e. higher energy) transmission electron microscope (TEM). The SEM has compensating advantages, though, including the ability to image a comparatively large area of the specimen; the ability to image bulk materials (not just thin films or foils); and the variety of analytical modes available for measuring the composition and properties of the specimen. Depending on the instrument, the resolution can fall somewhere between less than 1 nm and 20 nm. By 2009, the world's highest SEM resolution at high-beam energies (0.4 nm at 30 kV) is obtained with the Hitachi SU-9000.

AFM ANALYSIS

The AFM is one of the foremost tools for imaging, measuring, and manipulating matter at the nanoscale. The information is gathered by "feeling" the surface with a mechanical probe. Piezoelectric elements that facilitate tiny but accurate and precise movements on (electronic) command enable the very precise scanning. In some variations, electric potentials can also be scanned using conducting cantilevers.

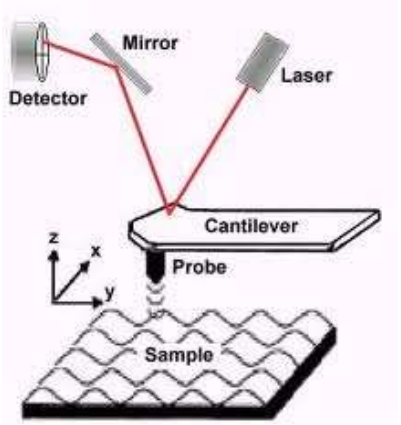

Fig 5. Schematic diagram of Atomic Force Microscope

The AFM consists of a cantilever with a sharp tip (probe) at its end that is used to scan the specimen surface. The cantilever is typically silicon or silicon nitride with a tip radius of curvature on the order of nanometers. When the tip is brought into proximity of a sample surface, forces between the tip and the sample lead to a deflection of the cantilever according to Hooke's law. Depending on the situation, forces that are measured in AFM include mechanical contact force, van der Waals forces, capillary forces, chemical bonding, electrostatic forces, magnetic force, Casimir forces, solvation forces, etc. Along with force, additional quantities may simultaneously be measured through the use of specialized types of probes. Typically, the deflection is measured using a laser spot reflected from the top surface of the cantilever into an array of photodiodes. Other methods that are used include optical interferometry, capacitive or piezo-resistive AFM cantilevers. These cantilevers are fabricated with piezo-resistive elements that act as a strain gauge. Using a Wheatstone, strain in the

INTERNATIONAL JOURNAL OF RESEARCH IN MECHANICAL, MECHATRONICS AND AUTOMOBILE ENGINEERING (IJRMMAE)
ISSN: 2454-1435 (Print) | 2454-1443 (online)
Volume 8 Issue 4, Jan. – Mar. 2023 - www.ijrmmae.in – Pages 1-15
Published On: 14th Feb 2023

AFM cantilever due to deflection can be measured, but this method is not as sensitive as laser deflection or interferometry. The AFM can be operated in a number of modes, depending on the applications.

CONTACT MODE

In contact mode, the tip is "dragged" across the surface of the sample and the contours of the surface are measured either using the deflection of the cantilever directly or, more commonly, using the feedback signal required to keep the cantilever at a constant position. Because the measurement of a static signal is prone to noise and drift, low stiffness cantilevers are used to boost the deflection signal. Close to the surface of the sample, attractive forces can be quite strong, causing the tip to "snap-in" to the surface. Thus, contact mode AFM is almost always done at a depth where the overall force is repulsive, that is, in firm "contact" with the solid surface below any adsorbed layers.

TAPPING MODE

In tapping mode, the cantilever is driven to oscillate up and down at near its resonance frequency by a small piezoelectric element mounted in the AFM tip holder similar to non-contact mode. However, the amplitude of this oscillation is greater than 10 nm, typically 100 to 200 nm. The interaction of forces acting on the cantilever when the tip comes close to the surface, Van der Waals forces, dipole-dipole interactions, electrostatic forces, etc. cause the amplitude of this oscillation to decrease as the tip gets closer to the sample. An electronic servo uses the piezoelectric actuator to control the height of the cantilever above the sample. The servo adjusts the height to maintain a set cantilever oscillation amplitude as the cantilever is scanned over the sample. An AFM image is therefore produced by imaging the force of the intermittent contacts of the tip with the sample surface.This method of "tapping" lessens the damage done to the surface and the tip compared to the amount done in contact mode. Tapping mode is gentle enough even for the visualization of supported lipid bilayers or adsorbed single polymer molecules under liquid medium.

NON-CONTACT MODE

In this mode, the tip of the cantilever does not contact the sample surface. The cantilever is instead oscillated at either its resonant frequency (frequency modulation) or just above (amplitude modulation) where the amplitude of oscillation is typically a few nanometers (<10 nm) down to a few picometers. The van der Waals forces, which are strongest from 1 nm to 10 nm above the surface, or any other long-range force that extends above the surface acts to decrease the resonance frequency of the cantilever. This decrease in resonant frequency combined with the feedback loop system maintains a constant oscillation amplitude or frequency by adjusting the average tip-to-sample distance. Measuring the tip-to-sample distance at each (x,y) data point allows the scanning software to construct a topographic image of the sample surface. Non-contact mode AFM does not suffer from tip or sample degradation effects that are sometimes observed after taking numerous scans with contact AFM.AFM used to study the surface morphology parameters such as Root Mean Square (RMS) roughness, Arithmetic average roughness and maximum peak height roughness, and so on.

$$\text{Root Mean Square Roughness } Rq=\sqrt{1/n[\sum_{i=1}^{n} yi^{2}]}$$

$$\text{Arithmetic average Roughness } Ra=1/n[\sum_{i=1}^{n} yi\,]$$

$$\text{Maximum Peak Height } Rp=\max y_i$$

INTERNATIONAL JOURNAL OF RESEARCH IN MECHANICAL, MECHATRONICS AND AUTOMOBILE ENGINEERING (IJRMMAE)
ISSN: 2454-1435 (Print) | 2454-1443 (online)
Volume 8 Issue 4, Jan. – Mar. 2023 - www.ijrmmae.in – Pages 1-15
Published On: 14th Feb 2023

Block on ring Test Method:

This test method covers the procedure for determining sliding wear of various materials using the block-on-ring geometry. A stationary block specimen is pressed with a constant force against a rotating ring specimen at 90º to the ring's axis of rotation. Friction between the sliding surfaces of the block and ring results in loss of material from both pieces. Many materials can be fabricated into blocks and rings, however the standard's emphasis is on metals. The test may be run at the loads, velocities, and temperatures which simulate the service conditions with various lubricants and liquid.

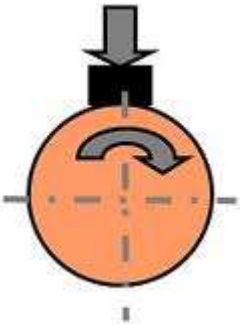

Fig 6. Schematic diagram of Block on ring Test Method

RESULTS AND DISCUSSION

RAMAN ANALYSIS

Raman spectroscopy is the best way to obtain the detailed bonding structures of DLC films. Fig 7. and Fig 8 shows the Raman spectra of as-deposited DLC film and Ti doped DLC film respectively. Both the Raman spectra exhibit a broad asymmetric peak in the range 1400–1700 cm^{-1}, which is typical of DLC films. The figure also shows some obvious differences between as-deposited DLC film and Ti-doped DLC film. The Raman spectrum of Ti-doped DLC film has the obvious shoulder peak at 1350 cm^{-1}.this peak indicative the Ti doped DLC structure.

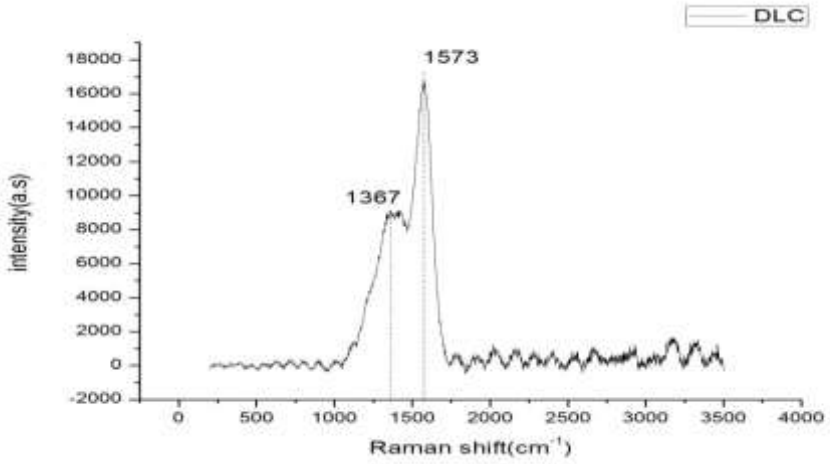

Fig 7. Raman spectrum of DLC

INTERNATIONAL JOURNAL OF RESEARCH IN MECHANICAL, MECHATRONICS AND AUTOMOBILE ENGINEERING (IJRMMAE)
ISSN: 2454-1435 (Print) | 2454-1443 (online)
Volume 8 Issue 4, Jan. – Mar. 2023 - www.ijrmmae.in – Pages 1-15
Published On: 14th Feb 2023

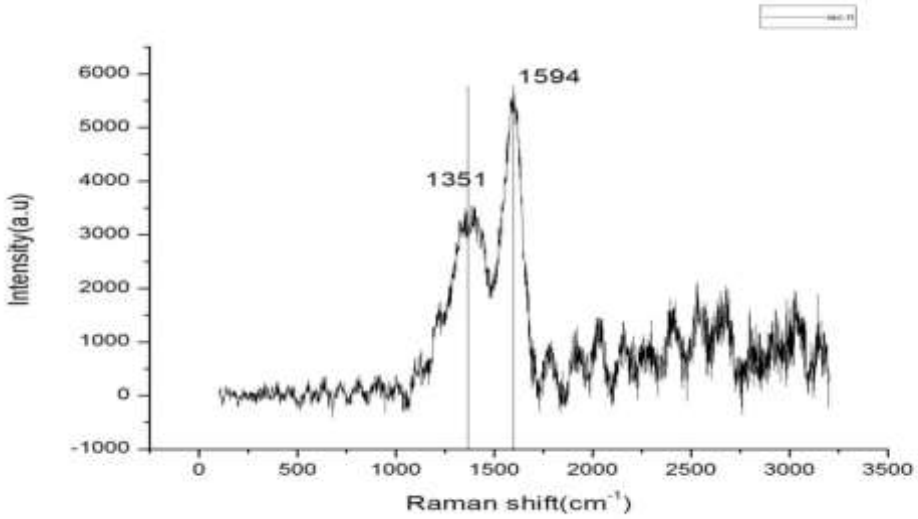

Fig 8. Raman spectrum of Ti-DLC

SEM ANALYSIS

SEM was used to study the surface morphology of the coated DLC and Ti-DLC In Fig 9. DLC image has nearly 1.2-1.8 micrometer diameter particles on the film surface which is in accordance with AFM results. In Fig 10. DLC-Ti image has nearly700-746 nm diameter particles on the film surface in this result also similar to the AFM result which agrees with the SEM observations. The doping of Ti on to DLC matrix may a reason for the shrinkage of grain size in the DLC matrix.

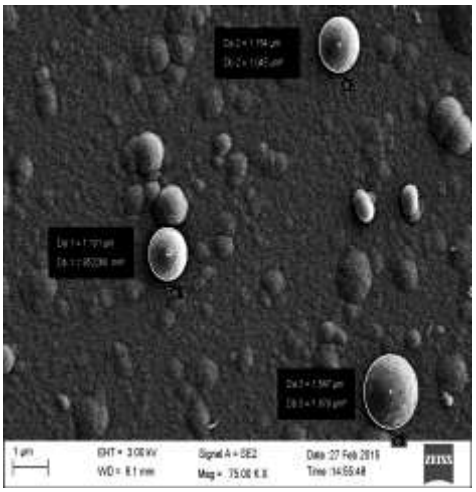

Fig 9. SEM image of DLC

INTERNATIONAL JOURNAL OF RESEARCH IN MECHANICAL, MECHATRONICS AND AUTOMOBILE ENGINEERING (IJRMMAE)
ISSN: 2454-1435 (Print) | 2454-1443 (online)
Volume 8 Issue 4, Jan. – Mar. 2023 - www.ijrmmae.in – Pages 1-15
Published On: 14th Feb 2023

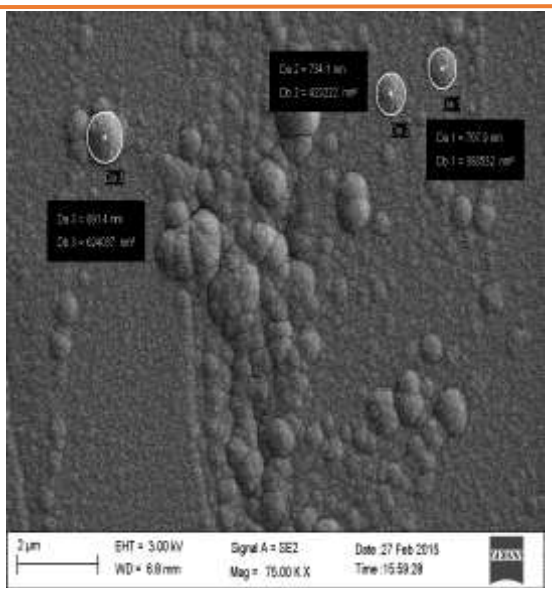

Fig 10. SEM image of Ti-DLC

The mainly EDAX is a semi quantitative method is used to find out the composition of the samples. In Fig 11 and Fig 12 shows the composition present in the DLC and Ti-DLC coated thin film respectively.

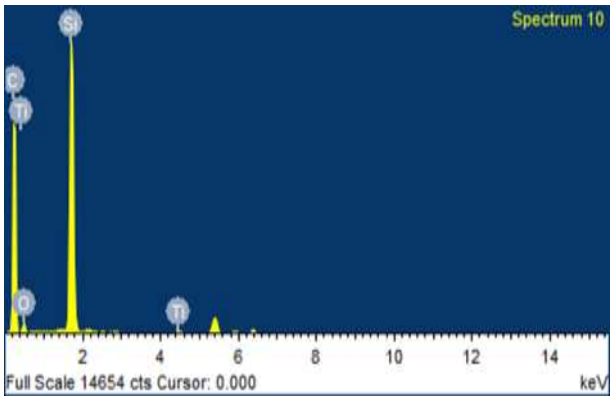

Element	Weight%	Atomic%
C K	82.86	90.53
O K	4.13	3.39
Si K	13.01	6.08
Totals	100	

Fig 11. Elements presents on the film surface as- sputtered DLC thin film EDAX spectrum and composition

INTERNATIONAL JOURNAL OF RESEARCH IN MECHANICAL, MECHATRONICS AND AUTOMOBILE ENGINEERING (IJRMMAE)
ISSN: 2454-1435 (Print) | 2454-1443 (online)
Volume 8 Issue 4, Jan. – Mar. 2023 - www.ijrmmae.in – Pages 1-15
Published On: 14th Feb 2023

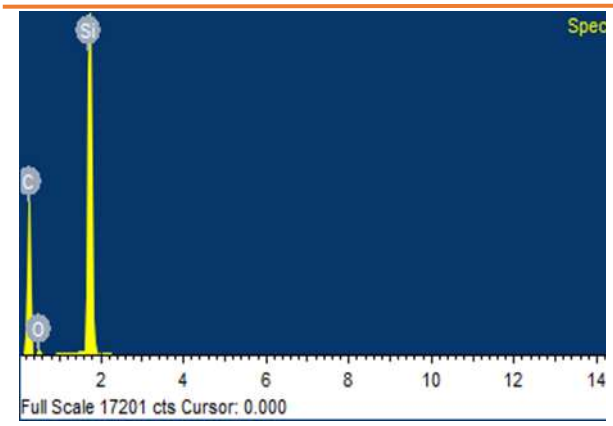

Element	Weight%	Atomic%
C K	83.77	90.34
O K	6.36	5.15
Si K	9.64	4.45
TiK	0.22	0.06
Total	100	

Fig 12. Elements presents on the film surface as- sputtered Ti-DLC thin film EDAX spectrum and composition

AFM ANALYSIS

The surface topography of 3D and topography image of as-sputtered DLC and DLC-Ti coated thin film are shown in Fig 13, 14 and Fig 16, 17. Topography image of the 25x25 micrometer area shows that a smooth surface is covered on the film surfaces. By the EDAX spectrum these bulk particle compositions were found to be the same as the target compositions and so these particles may be ejected from the target material during sputtering. Both the images show a smooth surface, but with bulk particles dispersed on the surface. Surface roughness parameters such as RMS roughness, and average roughness were calculated from the line profile across the imaged area. The Fig 15 and 18 shows that the roughness profile of the DLC and Ti-DLC sample respectively. Both the average roughness and RMS roughness is founded. Ti-DLC coated film roughness is high compare to the DLC coated thin film.

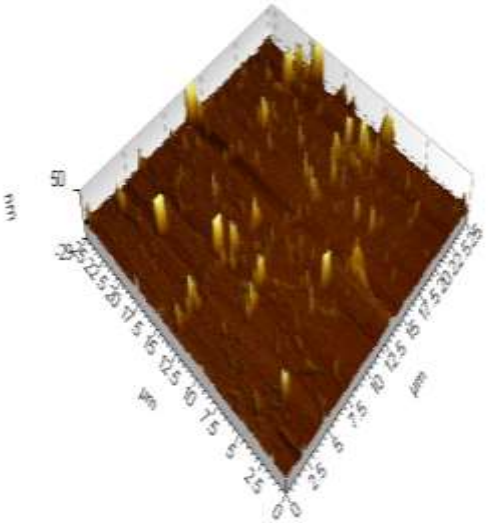

Fig 13. 3D image of DLC

INTERNATIONAL JOURNAL OF RESEARCH IN MECHANICAL, MECHATRONICS AND AUTOMOBILE ENGINEERING (IJRMMAE)
ISSN: 2454-1435 (Print) | 2454-1443 (online)
Volume 8 Issue 4, Jan. – Mar. 2023 - www.ijrmmae.in – Pages 1-15
Published On: 14th Feb 2023

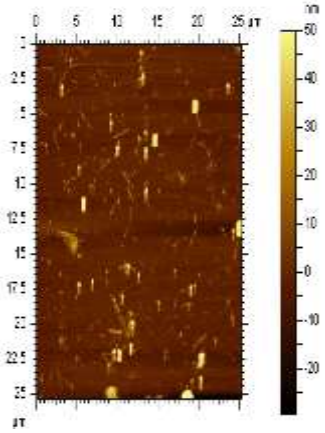

Fig 14. Topology image of DLC

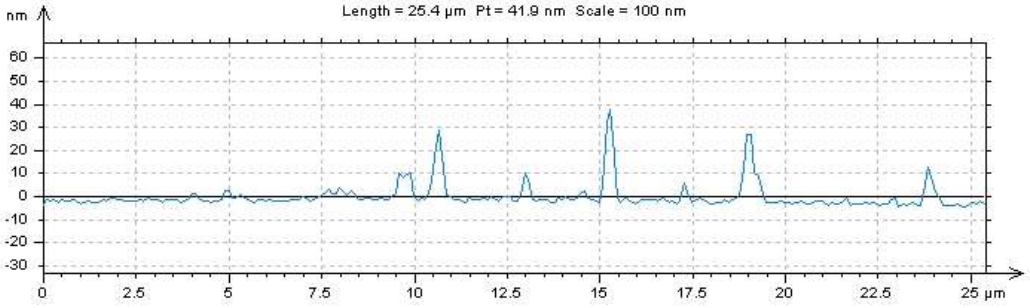

Fig 15. Roughness graph for 25x25 micrometer area DLC thin film

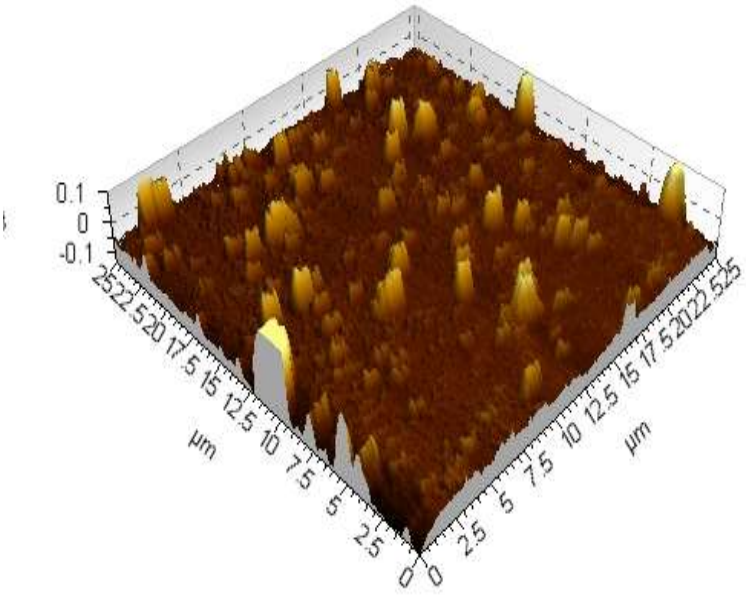

Fig 16. 3D image of Ti-DLC

INTERNATIONAL JOURNAL OF RESEARCH IN MECHANICAL, MECHATRONICS AND AUTOMOBILE ENGINEERING (IJRMMAE)
ISSN: 2454-1435 (Print) | 2454-1443 (online)
Volume 8 Issue 4, Jan. – Mar. 2023 - www.ijrmmae.in – Pages 1-15
Published On: 14th Feb 2023

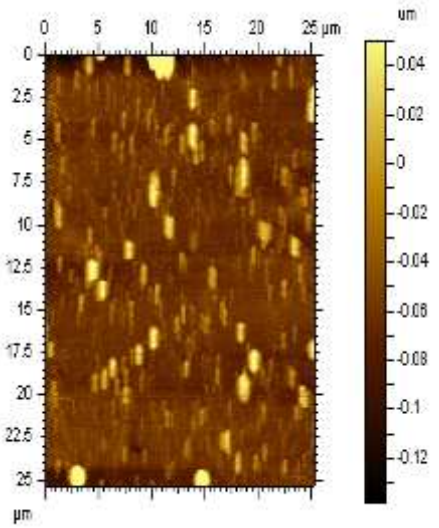

Fig 17. Topology image of Ti-DLC

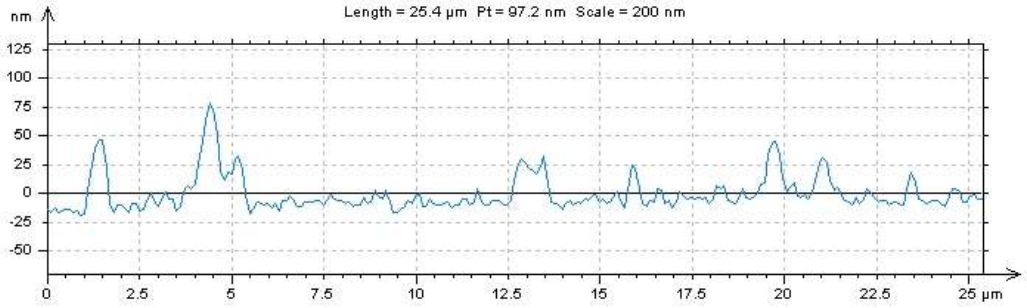

Fig 18. Roughness graph for 25x25 micrometer area Ti-DLC thin film

Coefficient of friction

Block on ring wear tester was used to find out the Coefficient Of Friction (COF) for DLC and Ti-DLC coated plate. In Fig 19.Comparisonbetween the DLC and Ti-DLC thin film. In this result Ti-DLC COF value is low compare to the DLC.

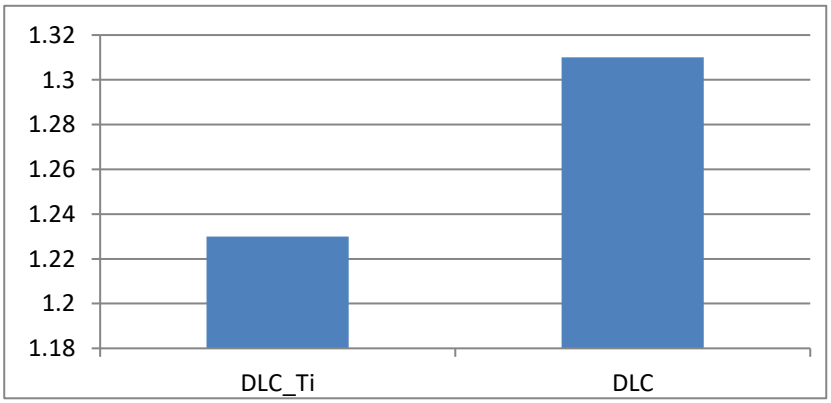

Fig 19. Friction coefficient of DLC and Ti doped DLC

INTERNATIONAL JOURNAL OF RESEARCH IN MECHANICAL, MECHATRONICS AND AUTOMOBILE ENGINEERING (IJRMMAE)
ISSN: 2454-1435 (Print) | 2454-1443 (online)
Volume 8 Issue 4, Jan. – Mar. 2023 - www.ijrmmae.in – Pages 1-15
Published On: 14th Feb 2023

QUALITATIVE EVALUATION OF DRILLING PERFORMANCE

The qualitative evaluation of coated drill to drill the SS plate was done to study the mechanical withstand limit of DLC and Ti-DLC. The fig 20 and 21 shows the Rapid I machine vision images before and after drilling the substrates with DLC coated drill bits and Ti-DLC coated drill bits. In this comparison, the Ti-DLC coated drill bit tip wear rate is low compare to the DLC coated drill bits.

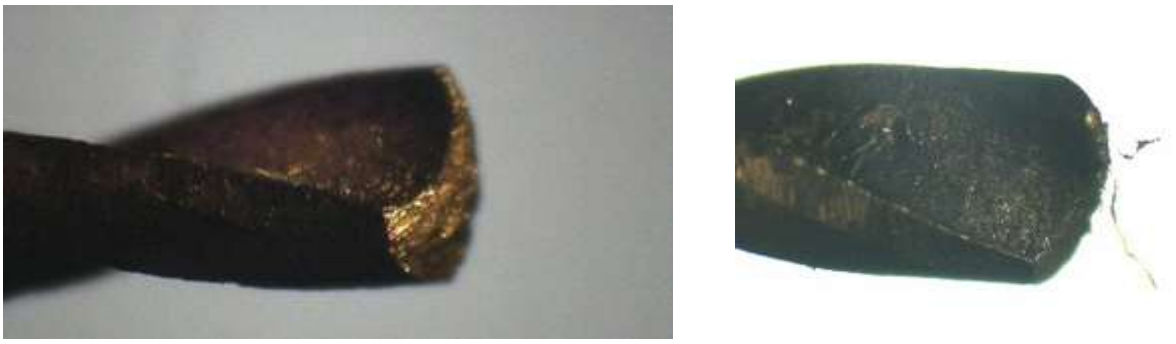

Fig 20. Machine vision image of DLC coated drill bits

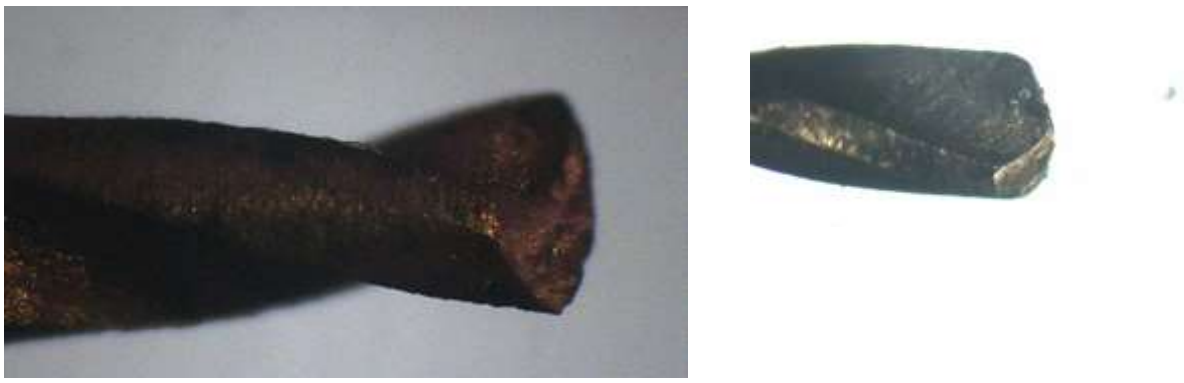

Fig 21. Machine vision image of DLC-Ti coated drill bits

Fig 22 shows the comparison for coated and uncoated drill bits performance. In this comparison diamond like carbon and Ti doped diamond like carbon coated drill bit operation performance is better compare to the uncoated drill bits performance.

INTERNATIONAL JOURNAL OF RESEARCH IN MECHANICAL, MECHATRONICS AND AUTOMOBILE ENGINEERING (IJRMMAE)
ISSN: 2454-1435 (Print) | 2454-1443 (online)
Volume 8 Issue 4, Jan. – Mar. 2023 - www.ijrmmae.in – Pages 1-15
Published On: 14th Feb 2023

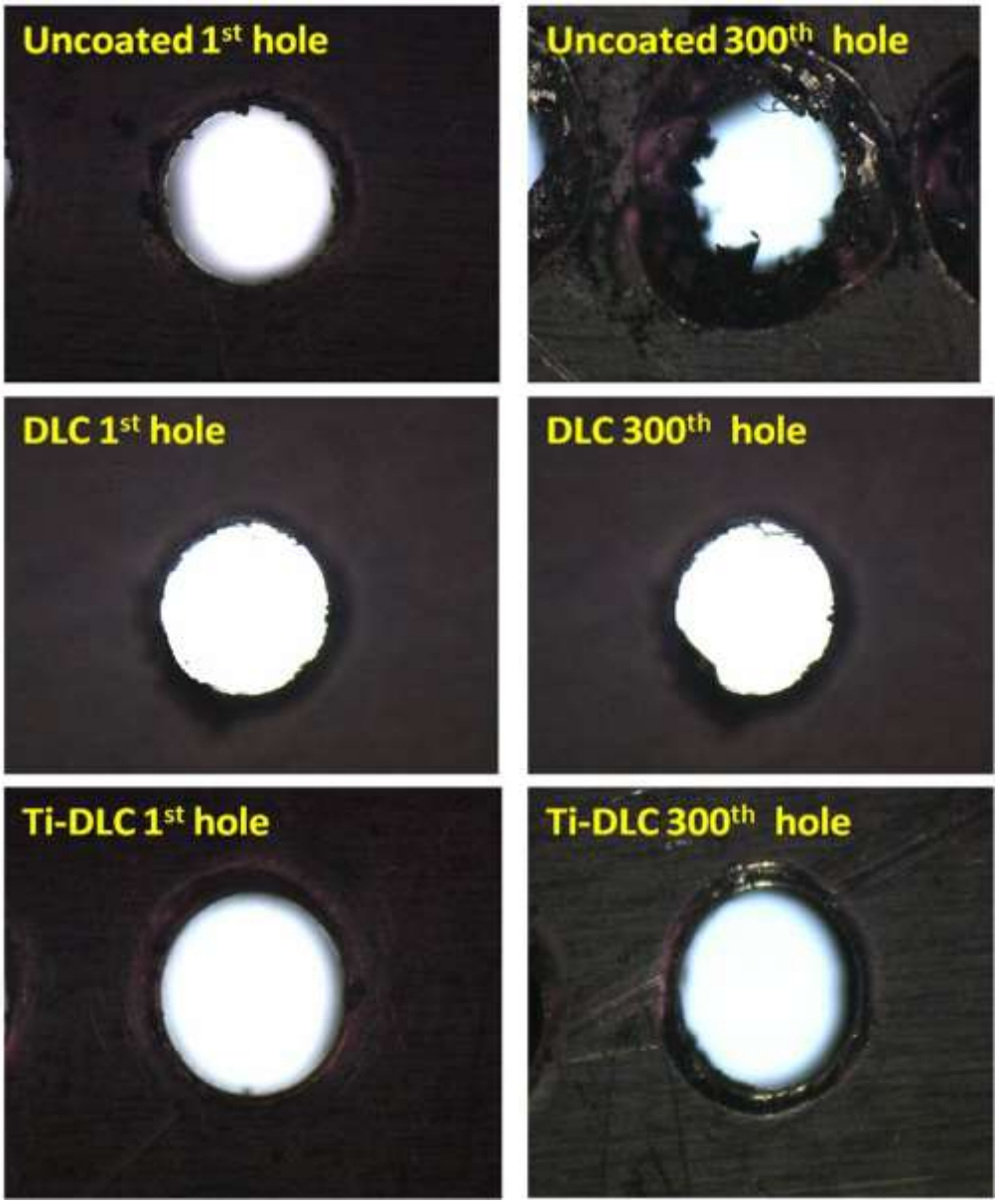

Fig 22. First hole for uncoated drilled (b)300th hole for uncoated drilled (c)first hole for dlc coated drilled (d)300th hole for DLC coated drilled (e)first hole for DLC-Ticoated drilled (f) 300th hole for DLC-Ti coated drilled.

CONCLUSION

The Raman spectrum of Ti-doped DLC film has the obvious shoulder peak at 1350 cm^{-1}which shows the peak indicative the Ti doped DLC structure. SEM observations shows that the doping of Ti on to DLC matrix may be a reason for the shrinkage of grain size in the DLC matrix. The average surface roughness of Ti-DLC coated film is high compare to the DLC coated thin film.The results show that the Coefficient of Friction of Ti-DLC value is low compare to the DLC. The machine vision images before and after drilling the substrates shows that the Ti-DLC coated drill bit tip

INTERNATIONAL JOURNAL OF RESEARCH IN MECHANICAL, MECHATRONICS AND AUTOMOBILE ENGINEERING (IJRMMAE)
ISSN: 2454-1435 (Print) | 2454-1443 (online)
Volume 8 Issue 4, Jan. – Mar. 2023 - www.ijrmmae.in – Pages 1-15
Published On: 14th Feb 2023

wear rate is low compare to the DLC coated drill bits.The results show that the Ti doped DLC coating has the optimal high-speed machining performance, i.e. it extends the tool life by a factor of at least four compared to the uncoated micro-drill and yields a significant improvement in the machining quality.

REFERENCES

1. Takadoum, J., Rauch, J. Y., Cattenot, J. M., & Martin, N. (2003). "Comparative study of mechanical and tribological properties of CNx and DLC films deposited by PECVD technique." Surface and Coatings Technology, Vol. 174, Pp. 427-433.
2. Park, Y. S., Myung, H. S., Han, J. G., & Hong, B. (2004). "Tribological properties of amorphous carbon thin films grown by magnetron sputtering method." *Surface and Coatings Technology*, Vol. *180*, Pp.218-221.
3. Corbella, C., Bertran, E., Polo, M. C., Pascual, E., & Andújar, J. L. (2007). Structural effects of nanocomposite films of amorphous carbon and metal deposited by pulsed-DC reactive magnetron sputtering. *Diamond and Related Materials*, *16*(10), 1828-1834.
4. Sedlaček, M., Podgornik, B., & Vižintin, J. (2008). Tribological properties of DLC coatings and comparison with test results: Development of a database. Materials Characterization, 59(2), 151-161.
5. Chen, J., Jia, J., Zhou, H., Chen, J., Yang, S., & Fan, L. (2008). Tribological behavior of short-fiber-reinforced polyimide composites under dry-sliding and water-lubricated conditions. *Journal of applied polymer science*, *107*(2), 788-796.
6. Zhao, F., Li, H., Ji, L., Wang, Y., Zhou, H., & Chen, J. (2010). Ti-DLC films with superior friction performance. *Diamond and Related materials*, *19*(4), 342-349.
7. Gayathri, S., Kumar, N., Krishnan, R., Ravindran, T. R., Dash, S., Tyagi, A. K., & Sridharan, M. (2012). Tribological properties of pulsed laser deposited DLC/TM (TM= Cr, Ag, Ti and Ni) multilayers. *Tribology International*, *53*, 87-97.
8. Guo, C. T., &Ueng, H. Y. (2014). Improved in dry routing performance with optimized diamond-like carbon films. *Vacuum*, *107*, 304-310.